Mixed convection in a driven cavity with a stable vertical temperature gradient

REIMA IWATSU

Institute of Computational Fluid Dynamics, 1-22-3 Haramachi, Meguro, Tokyo 152, Japan

JAE MIN HYUN

Korea Advanced Institute of Science and Technology, P.O. Box 150, Cheongryang, Seoul, Korea

and

KUNIO KUWAHARA

The Institute of Space and Astronautical Science, Yoshinodai, Sagamihara, Kanagawa, Japan

Abstract—Extensive parametric studies are made of flow and heat transfer of a viscous fluid contained in a square cavity. Flow is generated by the top horizontal boundary wall, which slides in its own plane at constant speed. A stabilizing externally-applied vertical temperature gradient is imposed on the system boundaries; the top wall is maintained at a higher temperature than the bottom wall. Numerical solutions to the Navier–Stokes equations are secured over broad ranges of the parameters, $0 \leqslant Ra \leqslant 10^6$, $0 \leqslant Re \leqslant 3000$, $Pr \sim O(1)$, aspect ratio $\sim O(1)$. Systematical evaluations of the numerical results are carried out to ascertain the relative importance of natural and forced convections. Representative plots illustrating the velocity and thermal fields are presented. These clearly identify the major dynamic elements in various regimes of the parameter spaces. When $Gr/Re^2 \leqslant 1$, the flow features are similar to those of a conventional driven-cavity of a non-stratified fluid. In the bulk of the interior, fluids are well mixed and temperature variations are small. When $Gr/Re^2 \gg 1$, much of the middle and bottom portions of the cavity interior is stagnant. In these regions, isotherms are nearly horizontal, and vertically-linear temperature distributions are seen. By inspecting separate plots of $\partial T/\partial y$ and $-Pr\,Re\cdot vT$, contributions to total heat transfer by conduction and by convection are assessed in a quantitative manner. The Nusselt number at the top wall is calculated, and these results indicate the intensification of heat transfer as $Gr/Re^2 \ll 1$.

1. INTRODUCTION

FLOW OF a viscous fluid contained in a rectangular cavity, with one of its boundary walls sliding at constant speed U_0, constitutes an appealing benchmark problem in numerical exercises. The geometry is straightforward and the boundary conditions are regular. The flow is characterized by two principal non-dimensional parameters, i.e. the Reynolds number, $Re = U_0 h/v$, and the cavity aspect ratio, $A \equiv h/W$, in which h and W are height and width of the cavity, and v is the kinematic viscosity of the fluid. Results of extensive numerical computational studies are available in the literature [1–9], and the consistency between these numerical predictions and laboratory experiments [3–5] has been explored [8, 9].

The introduction of a temperature gradient into the cavity boundaries produces an additional significant dynamical ingredient. The thermal non-homogeneity gives rise to buoyancy and this, in turn, impacts upon the coupled fields of velocity and temperature in the cavity. An understanding of this mixed forced–natural convective flow is of value from the standpoint of basic fluid dynamics as well as in practical engineering applications. A survey of the relevant literature,

however, reveals that studies of mixed convection within a closed cavity are relatively scarce.

Recently, Mohamad and Viskanta [10] reported the results of numerical investigations of mixed convective flow in a shallow cavity ($A \ll 1$). It should be noted that, in their analysis, the temperature at the top sliding surface, T_T, was lower than that at the stationary bottom surface, T_B. The two vertical side walls were thermally insulated. This created a gravitationally unstable flow configuration. The major elements of velocity and thermal characteristics were exhibited in the ranges of $200 \leqslant Re \leqslant 1000$ and $500 \leqslant |Ra| \leqslant 10^4$. Here, the buoyancy effect is measured by the Rayleigh number $|Ra|$, and the value of Ra may be interpreted to be negative as $\Delta T \equiv T_T - T_B < 0$. In particular, the computed results of this study illustrated the changes in the basic character of a gravitationally unstable configuration in a shallow cavity as Re and Ra encompassed the above-stated ranges.

As is evident in the non-dimensionalized governing equations, the fluid flow and accompanying heat transfer are characterized principally by four dimensionless parameters, i.e. Re, Gr, A and Pr. In the ensuing discussions, the aspect ratio is fixed to be

$A = 1.0$ (a square cavity), and the Prandtl number is set at $Pr = 0.71$ in most cases. This will allow evaluations of the explicit influences of forced convection (represented by Re) and of natural convection (typified by Gr). The ratio Gr/Re^2 emerges as a measure of the relative importance of natural convection to forced convection.

As pointed out earlier, the numerical work of Mohamad and Viskanta [10] was concerned with the cases when the externally-applied temperature difference was negative ($\Delta T < 0$), i.e. the bottom wall was heated. It is now proposed in the present endeavor to examine the flow and heat transfer properties in the cavity when the externally-imposed temperature difference leads to a gravitationally-stable configuration. Specifically, the top surface wall, which slides at constant velocity U_0, is maintained at temperature T_T, which is higher than the temperature at the stationary bottom wall, T_B, i.e. $\Delta T \equiv T_T - T_B > 0$. In contrast to the gravitationally unstable configuration of Mohamad and Viskanta [10], the system under present study will sustain a state of rest if the top surface wall is stationary. In this situation, heat transfer is entirely based on the conductive mode. However, the sliding motion of the top surface wall brings about fluid flows inside the cavity. Of primary interest is the effect of the stable stratification on the global flow and thermal fields. In practical terms, the augmentation of heat transfer rate, above that given by conduction alone, which is brought forth by forced convection, is of great significance. Stated alternatively, under a given imposed stable vertical temperature difference across the system, $\Delta T \equiv T_T - T_B$, the present investigation aims to delineate the heat transfer enhancement and the accompanying velocity field, which are achieved by forcing the top wall to slide in its own plane. In general, it is expected that, for a given value of Re, the stable stratification tends to inhibit vertical motions. Consequently, effective convective heat transfer is anticipated to decrease as the stable system-wide stratification intensifies.

In the present account, comprehensive numerical solutions were acquired to the complete Navier–Stokes equations using very fine grid meshes. Both the ranges of $|Ra|$ and Re were extended to cover the broader spectra of flow characteristics. Details of flow and thermal field structures will be depicted, and quantitative assessments will be made to portray the salient features in various parameter settings. The overriding motivation of this study is, as ascertained earlier, to demonstrate the substantial increase in global heat transfer above that given by the conductive mode. This is accomplished by forced convection, which is caused by the sliding top surface wall.

2. PROBLEM FORMULATION

The definition sketch of the problem is displayed in Fig. 1. The governing equations are the incom-
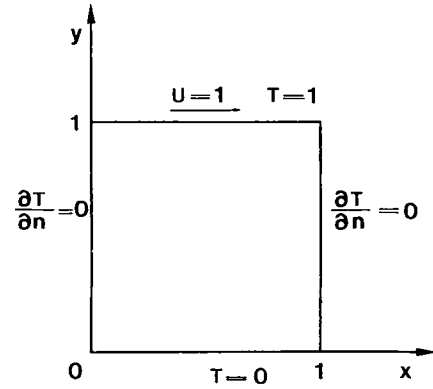

FIG. 1. Flow configuration and coordinate system.

pressible Navier–Stokes equations. The customary Boussinesq approximation is employed. These equations, expressed in properly non-dimensionalized form, are

$$\text{div } \mathbf{V} = 0 \tag{1}$$

$$\frac{\partial \mathbf{V}}{\partial t} + (\mathbf{V} \cdot \text{grad})\mathbf{V} = -\text{grad } p + Re^{-1} \Delta \mathbf{V}$$
$$+ Gr \cdot Re^{-2} T\mathbf{e} \tag{2}$$

$$\frac{\partial T}{\partial t} + (\mathbf{V} \cdot \text{grad})T = (Pr \cdot Re)^{-1} \Delta T, \tag{3}$$

where $\mathbf{V} = (u, v)$ is the velocity vector, p the pressure, T the temperature and $\mathbf{e} = (0, 1)$ a unit vector in the direction of the buoyancy force. In the above, the relevant dimensionless parameters are identified as:

$$Re = U_0 L/v$$
$$Ra = \beta \Delta T h^3/v\kappa$$
$$Pr = v/\kappa$$
$$Gr = Ra/Pr.$$

In accordance with the problem description, the boundary conditions are stated as:

$$\mathbf{V} = (1,0) \quad \text{at} \quad y = 1, \quad 0 \leqslant x \leqslant 1,$$
$$\mathbf{V} = 0 \quad \text{at} \quad x = 0, 1, \quad 0 \leqslant y \leqslant 1$$
$$\text{and} \quad y = 0, \quad 0 \leqslant x \leqslant 1,$$
$$T = 0 \quad \text{at} \quad y = 0, \quad 0 \leqslant x \leqslant 1,$$
$$T = 1 \quad \text{at} \quad y = 1, \quad 0 \leqslant x \leqslant 1,$$
$$\frac{\partial T}{\partial x} = 0 \quad \text{at} \quad x = 0 \quad \text{and} \quad x = 1, \quad 0 \leqslant y \leqslant 1.$$

The above system of equations is solved by resorting to a well-established finite difference numerical procedure. This numerical model represents an amended version of the MAC method [11–14]. Extensive model verifications have been documented as to the reliability and accuracy of this numerical

technique. For complete details, the reader is referred to the prior publications [15–17].

In order to test the spatial grid convergence, calculations were repeated using several different spatial resolutions, i.e. $\Delta x = \Delta y = 1/64$, $1/128$ and $1/256$ for $Re = 100$ and $Gr = 10^6$; and $\Delta x = \Delta y = 1/128$ and $1/256$ for $Re = 3000$ and $Gr = 10^6$. For these tests, $\Delta t = 0.005$, 0.002 and 0.001 for $\Delta x = \Delta y = 1/64$, $1/128$ and $1/256$, respectively. The outcome of these exercises indicated that the discrepancies in the computed velocity and temperature fields were less than 1%.

In summary, the above-stated sensitivity tests clearly demonstrated that the solutions are, to a fair degree of accuracy, independent of the grids and time intervals adopted in the present study. Consequently, in the numerical computations, Δx and Δy were chosen either as $1/128$ or $1/256$.

At the initial state, it is assumed that the fluid is motionless and a linear temperature stratification prevails throughout the whole domain. Calculations are continued until steady motion is attained. The transitory approach toward the steady state is not of primary concern here and it will not be treated in the present treatise.

3. RESULTS

As is immediately clear from the non-dimensionalized governing equations, the ratio Gr/Re^2 provides a measure of the importance of buoyancy-driven natural convection relative to lid-driven forced convection. If $Gr/Re^2 \ll 1$, the buoyancy effect is overwhelmed by the mechanical effect of the sliding lid. Therefore, as displayed in Fig. 2, the qualitative character of flow is similar to the conventional lid-

driven cavity flow of a non-stratified fluid. At high Reynolds numbers, the emergence of boundary layer-like flow features is apparent. These characteristics have been scrutinized in detail in preceding publications [8, 9].

As anticipated, the prominence of buoyancy effects is discernible throughout the cavity when $Gr/Re^2 \geqslant O(1)$. Figure 3, at $Gr = 10^6$, exemplifies this trend. In Fig. 3, curves (a) and (b) correspond to the cases $Gr/Re^2 \gg 1$. Due to the dominant influence of stabilizing buoyancy effects, the flows are almost stagnant in the bulk of the cavity interior, excluding the portions close to the sliding top wall. This typifies the flow structure which is stabilized by buoyancy-driven natural convection. It is stressed again that the present result is in contrast to the previous work of Mohamad and Viskanta [10], which dealt with a gravitationally unstable flow configuration. Curves (c) and (d) are characterized by $Gr/Re^2 \leqslant O(1)$; the qualitative velocity profiles are similar to those shown in Fig. 2, for which $Gr/Re^2 \ll O(1)$.

The numerical results are rearranged to demonstrate the change in basic flow character as Gr increases at a fixed Re, as displayed in Fig. 4. The changeover of the principal flow pattern is evident, as the criterion $Gr/Re^2 \leqslant O(1)$ is strongly satisfied (curves (a) and (b)) or not (curve (c)).

The global flow and temperature fields are depicted in Figs. 5 and 6. When the buoyancy effects are relatively small, $Gr/Re^2 \ll 1$, the gross flow features of Fig. 5 are similar to those of a conventional mechanically-driven cavity flow of a non-stratified fluid at comparable values of Re. The main circulation fills the entire cavity; minor cells are visible near the bottom corners. The isotherms are clustered close to the bottom lid, which points to the existence of steep tem-

```
***UMIN,UMAX,VMIN,VMAX
***1 -0.20370626 1.0000000 -0.24480307 0.16998208
***2 -0.31979227 1.0000000 -0.44589245 0.29554427
***3 -0.37819362 1.0000000 -0.51784348 0.36577463
***4 -0.42407644 1.0000000 -0.55746049 0.41593158
```
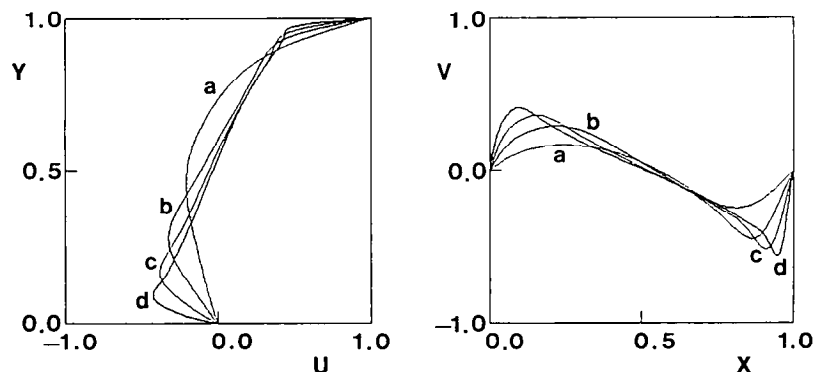

FIG. 2. Velocity profiles. (a) Profiles of horizontal velocity, u, along the vertical center line, $x = 0.5$. (b) Profiles of vertical velocity, v, along the horizontal midheight, $y = 0.5$. $Gr = 10^2$. The Reynolds numbers are: (a) $Re = 100$; (b) $Re = 400$; (c) $Re = 1000$; (d) $Re = 3000$.

```
***UMIN,UMAX,VMIN,VMAX
***1  -0.25125504  1.0000000   0.00000000E+00  3.59019265E-03
***2  -0.26322627  1.0000000  -8.97862948E-04  7.23083690E-03
***3  -0.17038333  1.0000000  -8.77381563E-02  9.69309211E-02
***4  -0.40658975  1.0000000  -0.54972339     0.40160173
```
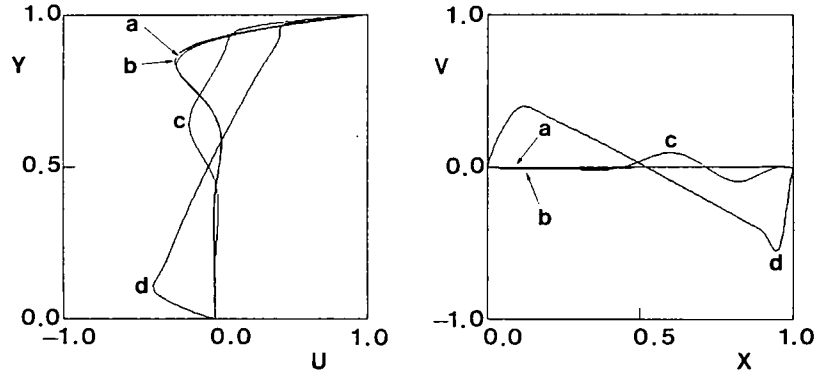
FIG. 3. Same as in Fig. 2 except for $Gr = 10^6$.

perature gradients in the vertical direction in this region. In the bulk of the cavity except this localized area, however, the temperature gradients are weak. This implies that, due to the vigorous actions of mechanically-driven circulations, fluids are well mixed; consequently, the temperature differences in much of this interior region are very small. On the other hand, when the buoyancy effects outweigh the effects of the sliding wall, i.e. $Gr/Re^2 \gg 1$, the flow and temperature fields are typified in Fig. 6. The interior circulation is restricted to a small zone close to the sliding top lid. The impact of the mechanically-driven top lid penetrates only small distances toward the interior region. Obviously, the stable stratification inhibits vertical motions; much of the fluid remains stagnant in the

middle and bottom interior regions. The vertical temperature stratification is substantially linear in the stagnant bulk of the interior regions. This reflects the fact that heat transfer is mostly conductive in the middle and bottom parts of the cavity. Only in a relatively small region in the top portion of the cavity are fluids comparatively well mixed; temperature is fairly uniform in this region, where the mechanically-induced convective activities are appreciable.

A systematic representation of the vertical temperature structures is portrayed in Fig. 7. Evidently, all the temperature profiles should satisfy the boundary conditions: $T = 0$ at $y = 0$ and $T = 1$ at $y = 1$. In the limit when the top lid is stationary, $Re \to 0$ or $Gr/Re^2 \gg 1$ at a finite Re, the interior fluid is motion-

```
***UMIN,UMAX,VMIN,VMAX
***1  -0.31979585  1.0000000  -0.44589722  0.29555106
***2  -0.30951858  1.0000000  -0.43180406  0.28371251
***3  -0.26322138  1.0000000  -8.97752121E-04  7.24285096E-03
```
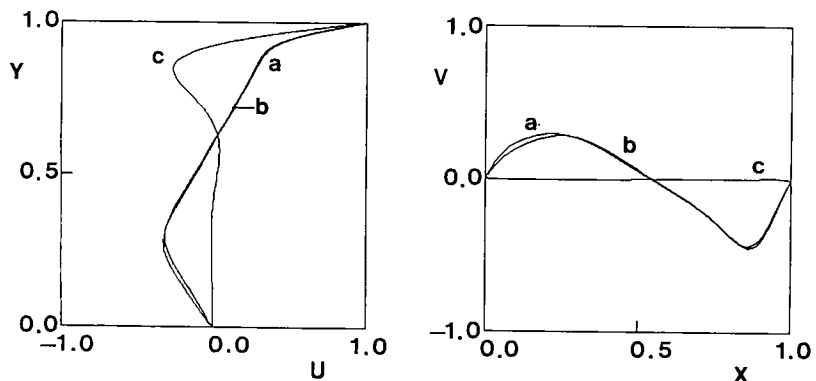
FIG. 4. Same as in Fig. 2. $Re = 400$. The Grashof numbers are: (a) $Gr = 10^2$; (b) 10^4; (c) 10^6.

ΓR:MIN,RMAX,LMAX -0.11521769 1.58714270E-03 2.56162835E-04 X,Y:MIN,RMAX,LMAX
.53307390 0.56809336 0.86770427 0.11673146 8.94941092E-02 8.56030583E-02 T,M
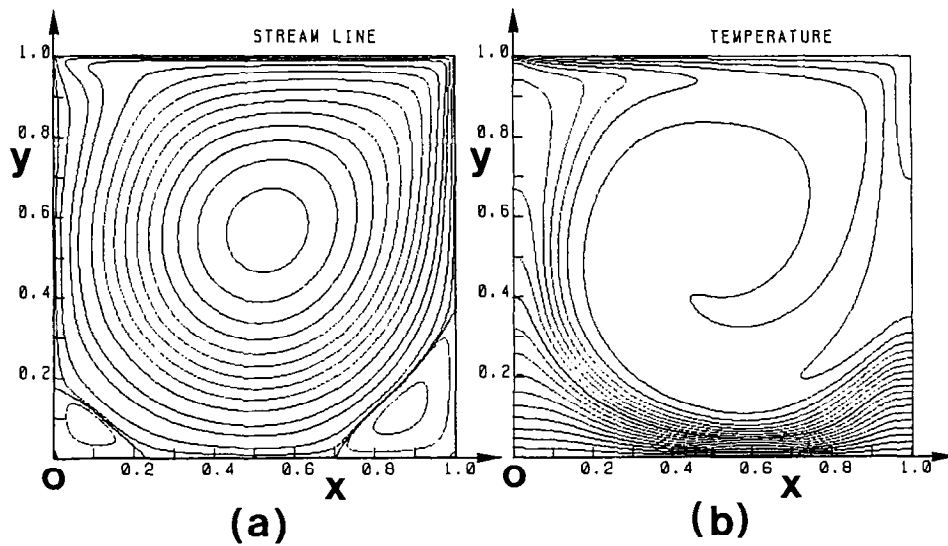√,MAX 0.00000000E+00 0.99785382

FIG. 5. Plots of the fields of velocity (a) and temperature (b). $Re = 10^3$, $Gr = 10^2$.

less and the corresponding temperature distribution approaches the linear profile obtained by the conduction solution. In the opposite case, when the buoyancy effect is minor, $Gr/Re^2 \ll 1$, much of the temperature variations is achieved in narrow strips adjacent to the top and bottom lids. In the middle portions of the cavity, the temperature changes are very small; as asserted earlier, these regions of near-uniform temperatures correspond to the areas in

which the mechanically-induced activities are appreciable.

The total vertical heat transport at a given height $y = y$ may be expressed as

$$\left[\frac{\partial T}{\partial y} - Pr\, Re \cdot vT \right]. \qquad (4)$$

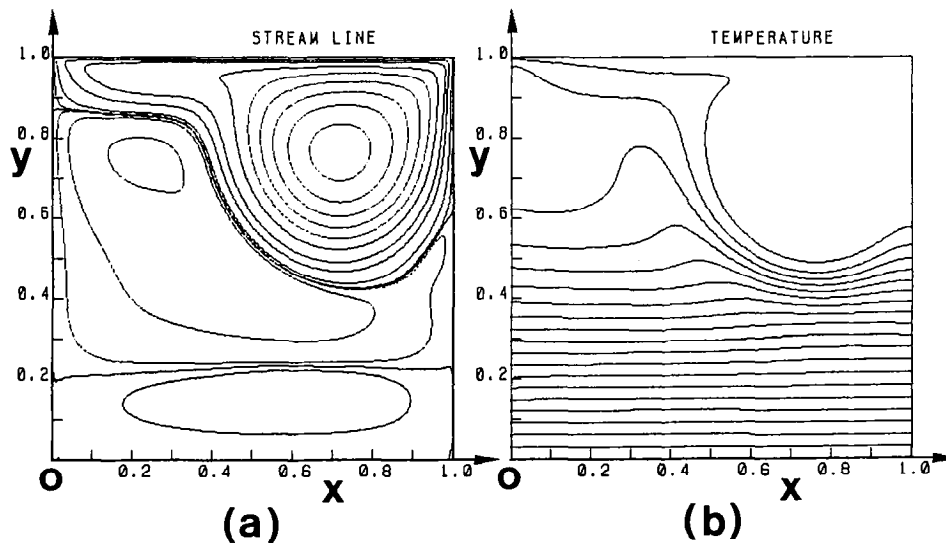In the above, the first and second terms denote the

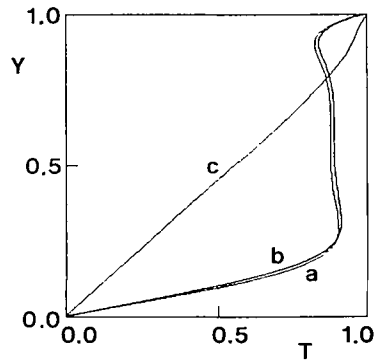FIG. 6. Same as in Fig. 5, except for $Re = 1000$, $Gr = 10^6$.

Fig. 7. Vertical temperature profiles along $x = 0.5$. $Re = 400$. The values of Gr are: (a) $Gr = 10^2$; (b) $Gr = 10^4$; (c) $Gr = 10^6$.
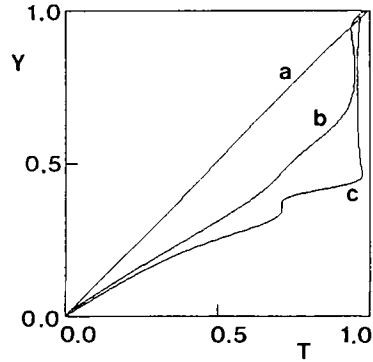

Fig. 9. Vertical temperature profiles along $x = 0.5$, $Re = 1000$, $Gr = 10^6$. The values of Pr are: (a) $Pr = 0.01$; (b) $Pr = 0.71$; (c) $Pr = 10.0$.

contributions attributable to conductive mode and convective mode, respectively. By inspecting separate plots of these two terms, the relative magnitude of each contribution may be appraised clearly. Figure 8 exemplifies such plots. Curve (c), for which $Gr/Re^2 \gg 1$, points to an overwhelming dominance of conduction, i.e. $\partial T/\partial y \rightarrow 1.0$ and $-Pr\,Re \cdot vT \sim 0$ over nearly the entire region of the cavity. On the other hand, when $Gr/Re^2 \leqslant O(1)$, the substantial contribution of convective heat transport, shown by the magnitudes of $-Pr\,Re \cdot vT$ in the middle and upper portions of the cavity is manifest. This scrutiny of the separate profiles of (4) reaffirms the qualitative trends discussed in the above.

Additional runs were made to inquire as to the effect of the Prandtl number Pr. Figure 9 exemplifies the qualitative aspects of the global temperature fields when $Gr/Re^2 \sim O(1)$. Clearly, when $Pr \ll 1$, the temperature distribution in the interior tends to the vertically-linear profile. This is demonstrative of the prevailing conductive heat transfer. When Pr is large, the upper part of the cavity interior is occupied by a strong circulatory cell, which renders a region of well-mixed fluids. Therefore, the vertical temperature pro-

file in the interior shows a zone of quite uniform temperature in the top portion of the cavity. However, in the bottom part of the cavity, the influence of the moving top boundary wall is relatively weak. The temperature distribution in this area illustrates a vertically-linear distribution, which reflects the prevalence of the conductive mode in this region.

Utilizing the wealth of computed results, the total heat transfer attainable at the top surface wall is calculated. This is represented by the Nusselt number $\overline{Nu}$, which is defined as

$$\overline{Nu} = \int_0^1 \left[\frac{\partial T}{\partial y}\right]_{y=1} dx. \tag{5}$$

The exemplary results of these calculations are contained in Table 1. Clearly, as $Gr/Re^2 \gg 1$, the domi-

Table 1. The Nusselt number $\overline{Nu}$ at the top wall

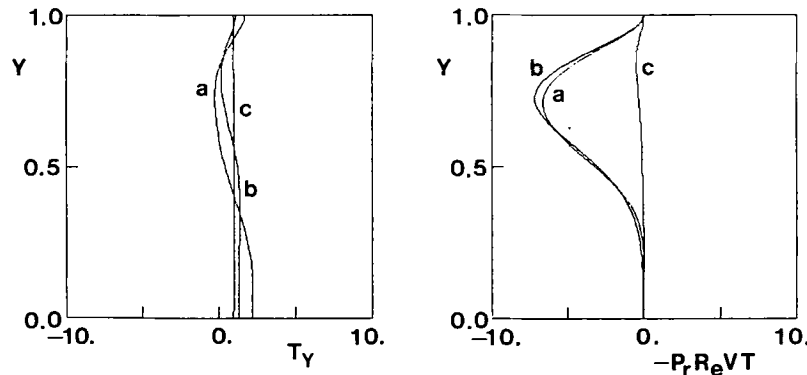| Re	$Gr = 10^2$	$Gr = 10^4$	$Gr = 10^6$
100	1.94	1.34	1.02
400	3.84	3.62	1.22
1000	6.33	6.29	1.77

Fig. 8. Vertical profiles of $\partial T/\partial y$ and $-Pr\,Re\,vT$ along $x = 0.5$. $Re = 100$. The values of Gr are: (a) $Gr = 10^2$; (b) $Gr = 10^4$; (c) $Gr = 10^6$.
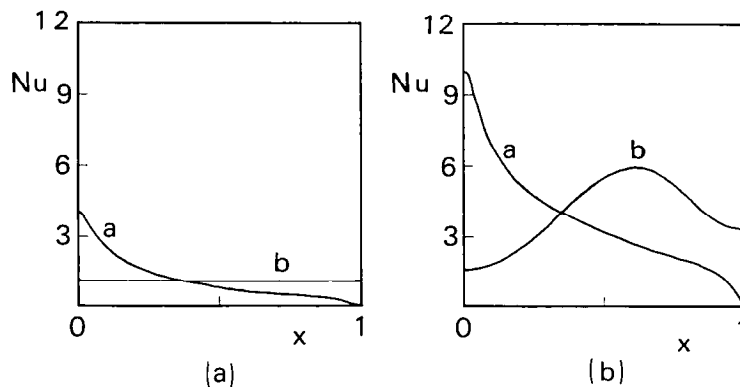
FIG. 10. Local Nusselt number profiles at the top and bottom walls. Profiles are along: (a) top wall, $y = 1.0$; (b) bottom wall, $y = 0.0$. (a) $Re = 400$, $Gr = 10^6$, $Pr = 0.71$. (b) $Re = 400$, $Gr = 100$, $Pr = 0.71$.

nance by conduction is obvious, and $\overline{Nu} \to 1.0$, accordingly. The intensification of heat transfer, induced by mechanically-driven forced convection, is apparent as $Gr/Re^2 \ll 1$.

The variations of local Nusselt number at the top and bottom walls are of interest in the practical design of heat transfer equipment. Figure 10(a) shows the results ($Re = 400$, $Gr = 10^6$, $Pr = 0.71$); the fluid motions are generally subdued and heat transport in the interior is dominated by conduction. Consequently, Nu at the bottom wall is close to unity. At the sliding top wall, owing to the presence of the circulation near the top left corner, convective heat transfer is appreciable. However, in the vicinity of the top right corner, the fluid temperature is fairly uniform in the vertical direction. Figure 10(b) portrays the local Nusselt number variations ($Re = 400$, $Gr = 100$, $Pr = 0.71$) when convective activities are dominant. The behavior of the Nusselt number profiles at both boundary walls clearly points to the existence of substantial fluid motions, leading to enhancement of heat transport throughout the cavity.

This baseline information is also useful to designers of practical heat exchangers. In addition, these numerical results will serve as reference materials against which further numerical or observational data may be compared.

4. CONCLUDING REMARKS

Numerical examinations are performed of mixed convective flow and heat transfer in a driven-cavity of aspect ratio $O(1)$. The effect of the mechanical drive of the top wall is represented by Re. A stabilizing externally-imposed vertical temperature differential, ΔT ($\equiv T_{top} - T_{bottom}$) > 0, is enforced on the system boundaries. The flow configuration is in contrast to that adopted in the previous study of Mohamad and Viskanta, who considered shallow, bottom-heated cavities.

When $Gr/Re^2 \ll 1$, the buoyancy effect is outweighed by forced convection, and the flow charac-

teristics are similar to those of a conventional lid-driven cavity of a non-stratified fluid. The isotherms are clustered only in narrow strips adjacent to the top and bottom walls. In the bulk of the central regions of the cavity, fluids are well mixed and temperature variations are very small.

Prominent buoyancy-driven convective features are discernible when $Gr/Re^2 \gg 1$. The direct effect of the sliding top wall penetrates only small distances into the interior region. Much of the middle and bottom portions of fluids is stagnant. In these near-stagnant regions, the isotherms are fairly horizontal and vertically-linear temperature distributions prevail. Only in small regions near the top sliding wall are fluids well mixed, and zones of fairly uniform temperature are noticeable.

The influence of Pr over the flow characteristics is studied for cases at $Gr/Re^2 \sim O(1)$. When Pr is low, the temperature field in the interior tends to a vertically-linear profile throughout the entire cavity. However, when Pr is high, the upper part of the cavity represents a region of well mixed fluids. The temperature field is fairly uniform in the upper portion of the cavity. In the bottom part of the cavity, the temperature distribution shows a vertically-linear profile.

Further inspections of the numerical results are corroborative of the qualitative features described in the above.

REFERENCES

1. U. Ghia, K. N. Ghia and C. T. Shin, High-Re solutions for incompressible flow using the Navier–Stokes equations and a multigrid method, *J. Comput. Phys.* **48**, 387–411 (1982).
2. R. Schreiber and H. B. Keller, Driven cavity flows by efficient numerical technique, *J. Comput. Phys.* **49**, 310–333 (1983).
3. J. R. Koseff and R. L. Street, Visualization studies of a shear driven three-dimensional recirculation flow, *J. Fluids Engng* **106**, 21–29 (1984).
4. J. R. Koseff and R. L. Street, On end wall effects in a

lid-driven cavity flow, *J. Fluids Engng* **106**, 385–389 (1984).

5. J. R. Koseff and R. L. Street, The lid-driven cavity flow: a synthesis of qualitative and quantitative observations, *J. Fluids Engng* **106**, 390–398 (1984).

6. C. J. Freitas, R. L. Street, A. N. Findikakis and J. Koseff, Numerical simulation of three-dimensional flow in a cavity, *Int. J. Numer. Meth. Fluids* **5**, 561–575 (1985).

7. C. Y. Perng and R. L. Street, Three-dimensional unsteady flow simulations: alternative strategies for a volume-averaged calculation, *Int. J. Numer. Meth. Fluids* **9**, 341–362 (1989).

8. R. Iwatsu, K. Ishii, T. Kawamura, K. Kuwahara and J. M. Hyun, Numerical simulation of three-dimensional flow structure in a driven-cavity, *Fluid Dyn. Res.* **5**, 173–189 (1989).

9. R. Iwatsu, J. M. Hyun and K. Kuwahara, Analyses of three-dimensional flow calculations in a driven cavity, *Fluid Dyn. Res.* **6**, 91–102 (1990).

10. A. A. Mohamad and R. Viskanta, Combined surface shear and buoyancy-driven convection in a shallow cavity, *Proc. AIAA/ASME Thermophysics and Heat Transfer Conf.* (1990).

11. F. H. Harlow and J. E. Welch, Numerical calculation of time-dependent viscous incompressible flow of fluid with free surface, *Phys. Fluids* **8**, 2182–2187 (1965).

12. K. Kawamura and K. Kuwahara, Computation of high Reynolds number flow around a circular cylinder with surface roughness, AIAA paper 84-0340 (1984).

13. H. A. Van der Vorst, Bi-CGSTAB: a fast and smoothly converging variant of Bi-CG for the solution of non-symmetric linear systems, *SIAM J. Sci. Statist. Comput.* **13**(2), 631–644 (1992).

14. S. Fujino, Visualization of convergence behavior of Bi-CGSTAB method, *Proc. Int. Symp. on Computer Arithmetic and Scientific Computation* (1991).

15. R. Iwatsu, J. M. Hyun and K. Kuwahara, Numerical simulation of torsionally-oscillating lid in a square cavity, *J. Fluids Engng* **114**, 143–151 (1992).

16. R. Iwatsu, J. M. Hyun and K. Kuwahara, Convection in a differentially-heated square cavity with a torsionally-oscillating lid, *Int. J. Heat Mass Transfer* **35**, 1069–1076 (1992).

17. R. Iwatsu, J. M. Hyun and K. Kuwahara, Flows driven by a torsionally-oscillating lid in a square cavity with stable stratification, AIAA paper 91-0163 (1991).